

See discussions, stats, and author profiles for this publication at: <https://www.researchgate.net/publication/236931703>

# The FMO Complex in a Glycerol-Water Mixture

ARTICLE *in* THE JOURNAL OF PHYSICAL CHEMISTRY B · MAY 2013

Impact Factor: 3.3 · DOI: 10.1021/jp311380k · Source: PubMed

---

CITATIONS

13

---

READS

63

## 5 AUTHORS, INCLUDING:



**Mortaza Aghtar**

Jacobs University

9 PUBLICATIONS 131 CITATIONS

[SEE PROFILE](#)



**Carsten Olbrich**

Jacobs University

15 PUBLICATIONS 385 CITATIONS

[SEE PROFILE](#)



**Ulrich Kleinekathöfer**

Jacobs University

117 PUBLICATIONS 2,057 CITATIONS

[SEE PROFILE](#)

# The FMO Complex in a Glycerol–Water Mixture

Mortaza Aghtar,<sup>†,||</sup> Johan Strümpfer,<sup>‡,||</sup> Carsten Olbrich,<sup>†</sup> Klaus Schulten,<sup>‡,§</sup> and Ulrich Kleinekathöfer<sup>\*,†</sup>

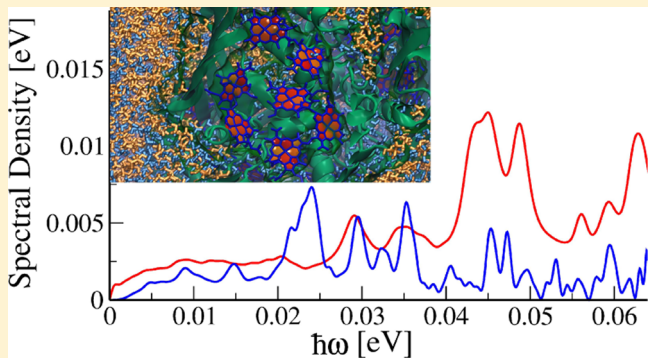
<sup>†</sup>School of Engineering and Science, Jacobs University Bremen, Campus Ring 1, 28759 Bremen, Germany

<sup>‡</sup>Center for Biophysics and Computational Biology and Beckman Institute, University of Illinois at Urbana–Champaign, Urbana, Illinois 61801, United States

<sup>§</sup>Department of Physics, University of Illinois at Urbana–Champaign, Urbana, Illinois 61801, United States

 Supporting Information

**ABSTRACT:** Experimental findings of long-lived quantum coherence in the Fenna–Matthews–Olson (FMO) complex and other photosynthetic complexes have led to theoretical studies searching for an explanation of this unexpected phenomenon. Extending in this regard our own earlier calculations, we performed simulations of the FMO complex in a glycerol–water mixture at 310 K as well as 77 K, matching the conditions of earlier 2D spectroscopic experiments by Engel et al. The calculations, based on an improved quantum procedure employed by us already, yielded spectral densities of each individual pigment of FMO, in water and glycerol–water solvents at ambient temperature that compare well to prior experimental estimates. Due to the slow solvent dynamics at 77 K, the present results strongly indicate the presence of static disorder, i.e., disorder on a time scale beyond that relevant for the construction of spectral densities.



Excitation energy transfer is of key importance in many natural as well as artificial systems performing photosynthesis. In green sulfur bacteria, and some other phototrophs, large vesicles of pigments, called chlorosomes, act as primary antennae for capturing light. In these systems, an excitation energy transfer connection between the chlorosomes and the reaction center, in which light energy absorbed is utilized for charge separation, is provided by the Fenna–Matthews–Olson (FMO) complex.<sup>1</sup> The crystal structure of this complex has been known for some time;<sup>2</sup> high-resolution structures for the reaction center from *Prosthecochloris aestuarii*<sup>3</sup> and *Chlorobaculum tepidum*<sup>4</sup> were reported more recently. Under physiological conditions, the FMO complex forms a homotrimer with each monomer containing eight bacteriochlorophyll-*a* (BChl *a*) molecules (see Figure 1). In many spectroscopic experiments, however, the monomers seem to contain only seven pigments, most likely as a result of sample preparation procedures.

More than five years ago, the first long-lived coherence effects in biology were observed using time-resolved optical two-dimensional spectra<sup>5–7</sup> and prompted many theoretical investigations trying to find an explanation for these unexpected effects. Later on, similar effects were observed for a photosynthetic complex found in marine algae at ambient temperature<sup>8</sup> as well as in conjugated polymers.<sup>9</sup> Several questions arose in connection with these experiments: How can quantum coherence survive for a picosecond in a biological system (even at low temperatures)? Can quantum coherence be used to enhance excitation transfer in artificial systems? Does quantum coherence have any functional importance for biological

photosynthesis? There have been many investigations attempting to answer the first two questions.<sup>10–20</sup> A few studies have reported atomistic simulations, similar to those reported herein, attempting to address the first two questions.<sup>21–27</sup> Here we report simulations of FMO from *Chlorobaculum tepidum* in a glycerol–water solvent, in the same ratio as earlier experiments,<sup>6</sup> at 310 and 77 K. The simulations are used as input to an improved procedure, compared to earlier studies,<sup>21–24</sup> to determine spectral densities that compare well with earlier experimental estimates.<sup>28</sup>

Since the nonlinear experiments are performed on ensembles of FMO molecules, in simulations one either has to perform density matrix calculations using spectral densities or ensemble-averaged wave packet simulations. To obtain the spectral densities, key ingredients for dissipative quantum dynamics calculations,<sup>29,30</sup> we follow a procedure outlined earlier. In this scheme a combination of ground-state molecular dynamics (MD) simulations, electronic structure calculations along the classical trajectory, and a final extraction of the spectral density is employed.<sup>23,31,32</sup> The details of the MD simulations using the FMO trimer from *Chlorobaculum tepidum* (PDB code: 3ENI) immersed in water at 300 K have been detailed earlier.<sup>22,23</sup> The simulations of FMO in the 65% glycerol and 35% water solvent employed glycerol parameters from ref 33. A prior study

**Received:** November 18, 2012

**Revised:** May 22, 2013

**Published:** May 23, 2013



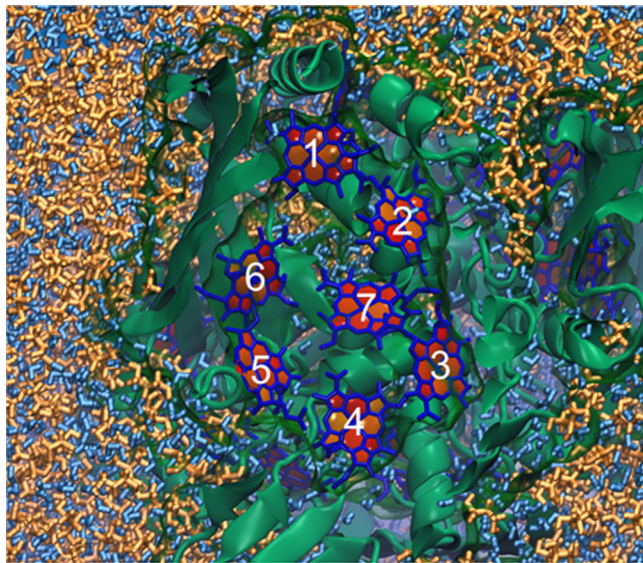


**Figure 1.** Monomer of the FMO trimer with the protein structure shown in cartoon representation and the labeled BChls in blue and red. The surrounding glycerol is displayed in yellow, and the water in light blue. The front part of the protein has been removed to make the BChls visible. BChl 8 is hidden behind BChl 1.

analyzing glycerol–water mixtures using MD simulations was reported recently.<sup>34</sup> The FMO in glycerol–water solvent was assembled and equilibrated for 10 ns at 310 K. Moreover, the systems with water and the glycerol–water mixture as solvents were cooled in eight steps of 3 ns down to 77 K. Subsequent to equilibration, the systems were propagated for 300 ps and snapshots were saved every 5 fs, i.e., 60 000 snapshots were produced for each of the four simulation setups.

The experiments leading to the observation of long-lived coherence in FMO<sup>5–7</sup> were conducted in 65% glycerol and 35% aqueous solution, which also contains 0.1% by mass lauryldimethylamine oxide (LDAO), which is known to form micelles around the proteins in the solution.<sup>6,7</sup> LDAO was not added in the present simulation, so that a possible formation of micelles around the protein was not considered at present. Therefore, the solvent fluctuations might be overestimated in the present investigation compared to experiment. Furthermore, one has to keep in mind that in the present ground-state MD simulations, nonpolarizable force fields are employed that may underestimate electrostatic screening.

The energy gap between the BChl ground and first excited state, i.e., the BChl  $Q_y$ , along the ground-state MD simulation were determined for each BChl. As in earlier studies<sup>22,23,32</sup> this was done using the ZINDO/S-CIS approach (Zerner Intermediate Neglect of Differential Orbital method with parameters for spectroscopic properties together with the configuration interaction scheme using single excitations only). The advantages and limitations of this approach have been discussed earlier,<sup>22,32,35</sup> but it has been shown to treat environmental effects in chromophores more accurately than, e.g., density functional-based approaches.<sup>36</sup> Of key importance is the quantum mechanics/molecular mechanics (QM/MM) treatment: each BChl is treated separately with the environment taken into account by including all the partial charges in the force field. We employed the approach outlined in ref 37 and implemented in the ORCA code.<sup>38</sup> In previous calculations, we included partial charges within a 20 Å radius

around the pigment. Though the distribution of energy gaps converged with this cutoff radius, extended studies on spectral densities showed a clear effect of the radius on the low frequency energy gap oscillations. Therefore, the procedure was modified to include all partial charges in the system. Due to the periodic boundary conditions in the MD box, one can redefine the box such that the BChl of interest is in its center. All partial charges in this box other than those from the BChl itself are included in the QM/MM calculation. The charges from the periodic images are not considered, which makes the redefinition of the box before each QM/MM calculation necessary. Using this modified procedure, spurious effects from charges entering or leaving the considered MM region are minimized. Enlarging the box size showed no significant effect. The ambient temperature distributions of energy gaps, also called site energies, for the individual BChls are shown in Figure 2. The site energy distributions at room temperature are

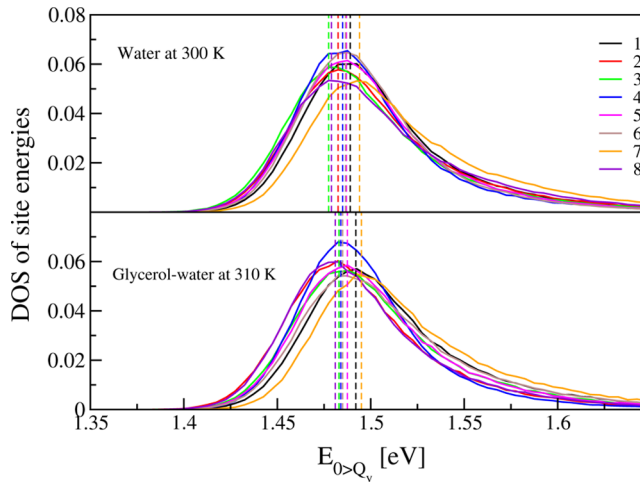


**Figure 2.** Distributions of energy gaps for individual pigment molecules at room temperature. The dashed lines indicate the peak positions of the distributions.

very broad compared to the splitting of the peak positions. Only small differences between the site energy distributions of FMO in the pure water solvent and the glycerol–water mixture can be seen at this temperature. The situation at 77 K is different. As expected, the thermal fluctuations shown in Figure 3 are reduced considerably at 77 K. The most striking feature of this low-temperature data is that for several BChls, the density of states (DOS) varies between the different monomers within one FMO trimer. At room temperature, there is only a very small variation, and it was therefore easily possible to determine an average DOS over monomers. At 77 K, however, such an averaging procedure is not easily feasible. Some very slow fluctuations with time scales longer than that of our trajectories, cannot easily be incorporated in our analysis. Redoing the same quantum chemistry analysis after some additional MD equilibration or, e.g., running a slightly different MD cooling protocol, the results are varying to some degree. The simulations were repeated several times partly including a complete resolution of the protein. Furthermore, simulations with different ionic strengths and different sizes of water boxes were performed to ensure that the static disorder seen in the low-temperature simulations is not a simulation artifact. In all these tests we encountered varying DOS distributions and spectral densities for the BChls in the different monomers. For

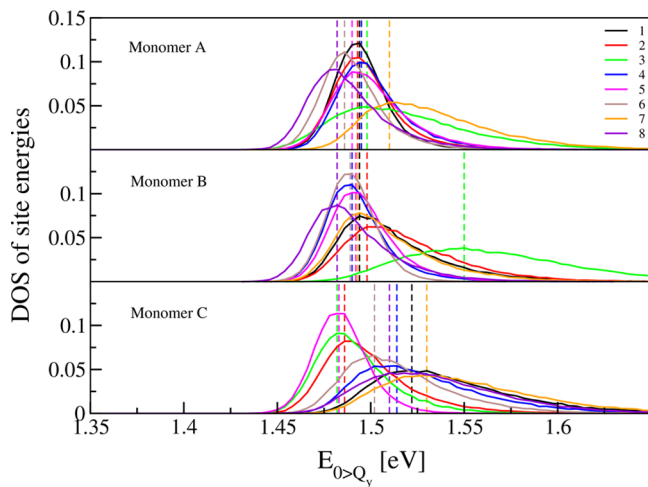


**Figure 3.** Example distributions of energy gaps for individual pigment molecules at 77 K. Especially the peak positions show disorder due to the slow fluctuations at low temperatures. The dashed lines indicate the peak positions of the distributions.

each of these simulations the variations in the DOS and spectral densities were unpredictable but of the same order of magnitude. At the same time, we cannot completely rule out that extremely long equilibration runs may lead to more symmetric solvent arrangements with respect to the monomers. Specialized simulation setups might also lead to symmetric conformations, although it is unclear if these are statistically the most relevant conformations. Analyzing the present MD trajectories one realizes, e.g., that at 77 K the water molecules around the protein basically do not move but only vibrate at their positions during the period of our QM analysis, i.e., during trajectories of length of 300 ps. At the same time, inspection of the hydrogen bond network in the water or the glycerol–water mixture shows very little changes. This is quite different in the room temperature results in which hydrogen bonds are constantly formed and broken since the solvent molecules are moving and rotating much more than at 77 K. This movement of the solvent molecules and also the protein atoms lead to an averaging procedure. Therefore, at ambient temperatures, no significant differences in the DOS of the different monomers are visible. In the 77 K simulations, this additional averaging happens on much longer time scales and therefore leads to static disorder. As a consequence of these findings, we will mainly analyze the room-temperature data to obtain spectral densities but will also comment on the differences found at low temperatures. In the study by Shim et al.<sup>25,27</sup> simulations at 77 and 300 K were compared for the case of a single monomer in water. Interestingly, the spectral densities for the FMO of *Prosthecochloris aestuarii* showed very little temperature dependence (see also discussion below).

For the ambient temperature simulations, Table 1 lists the peak position and average energies for the individual BChl distributions. Due to the asymmetry of the distributions, these values do differ considerably for some of the pigments, especially BChl 7. Since the parametrization of the ZINDO/S approach has been performed for conformations close to equilibrium, the accuracy of the results at the far ends of the distributions is unclear and needs more testing with higher-accuracy approaches. Therefore the peak values might be as meaningful as the averages when discussing the site energies. For the

**Table 1. Peak Postions and Average Energies of the Energy Gap DOSS**

	water 300 K		glycerol 310 K	
	peak [eV]	average [eV]	peak [eV]	average [eV]
1	1.489	1.509	1.492	1.515
2	1.482	1.505	1.483	1.498
3	1.480	1.450	1.483	1.506
4	1.483	1.450	1.484	1.499
5	1.485	1.502	1.487	1.507
6	1.486	1.501	1.485	1.512
7	1.492	1.522	1.495	1.524
8	1.482	1.510	1.481	1.499

glycerol–water mixture at 310 K, the peak position of site 8 is lowest but sites 2 and 3 are very close in energy. In the case of the average, BChl 2 has the lowest energy. We do not list any data for the 77 K simulations because of the problems with the very slow fluctuations. One would have to perform many simulations of the type performed in this study, starting from slightly different conditions, to obtain reasonable values for the peak and average positions at 77 K.

In theories describing dissipative effects in quantum systems, one usually splits the total Hamiltonian  $H$  into a system part  $H_S$ , a bath part  $H_B$ , and a coupling between the system and bath. Denoting the system operator describing pigment  $j$  by  $K_j$  and the system-bath coupling operator by  $\Phi_j$ , the total Hamiltonian can be written as

$$H = H_S + H_B + \sum_j K_j \Phi_j = H_S + H_B + \sum_j K_j \sum_\xi c_{j\xi} x_\xi \quad (1)$$

Here we assume linear coupling to the bath modes  $x_\xi$  with coupling constants  $c_{j\xi}$ . Using the notation  $m_\xi$  for the mass of the bath oscillator  $\omega_\xi$ , the spectral density of pigment  $j$  embedded in a harmonic bath is given by

$$J_j(\omega) = \frac{\hbar}{\pi} J_{CL,j}(\omega) = \frac{1}{2} \sum_\xi \frac{c_{j\xi}^2}{m_\xi \omega_\xi} \delta(\omega - \omega_\xi) \quad (2)$$

where  $J_{CL,j}(\omega)$  is the spectral density in the Caldeira–Legett model that differs from the present definition by a constant factor.

The spectral density  $J_j(\omega)$  describes the frequency-dependent coupling of pigment  $j$  to the thermal environment. Denoting the inverse temperature by  $\beta = 1/(k_B T)$  and the bath correlation function by  $C_j(t)$ , the spectral density  $J_j(\omega)$  of BChl  $j$  can be expressed by<sup>31,39</sup>

$$J_j(\omega) = \frac{2}{\pi \hbar} \tanh(\beta \hbar \omega / 2) \int_0^\infty dt C_j(t) \cos(\omega t) \quad (3)$$

which is the key relation for combining the results from MD and quantum chemistry calculations with dissipative exciton dynamics.

Here we wish to mention an inconsistency that arises while deriving eq 3, as also discussed by Valleau et al.<sup>27</sup> In deriving eq 3, the real part of the quantum mechanical correlation function has been replaced by its classical high-temperature counterpart. In the prefactor, however, the high-temperature limit has not been performed leading to the aforementioned inconsistency. Taking the high-temperature limit for the prefactor leads to

$$J_j(\omega) = \frac{\beta\omega}{\pi} \int_0^\infty dt C_j(t) \cos(\omega t) \quad (4)$$

As has been shown by Valleau et al.<sup>27</sup> this latter expression leads to spectral densities that are rather temperature-independent as opposed to the results using eq 3.

The energy gap fluctuations  $\Delta E_{j,l}(t_i)$  need to be computed at time steps  $t_i$  for BChl  $j$  in monomer  $l$ . For symmetry reason we average over the equivalent pigments in the three monomers of the FMO trimer. The discrete autocorrelation function  $C_j(t_i)$  is then given by<sup>31</sup>

$$C_j(t_i) = \frac{1}{3} \sum_{l=1}^3 \left[ \frac{1}{N-i} \sum_{k=1}^{N-i} \Delta E_{j,l}(t_i + t_k) \Delta E_{j,l}(t_k) \right] \quad (5)$$

where  $N$  denotes the number of time points taken into account. Analyzing the site energy fluctuation, we find that the fastest oscillations have periods of around 20 fs<sup>22,23,32</sup> attributed to vibrational motions including C=C and C=O double bonds.<sup>31,40,41</sup> Therefore we utilized a time step of 5 fs between the individual snapshots of the MD and ZINDO/S calculations leading to 60 000 snapshots (300 ps) per simulated system. With 24 QM/MM calculations for the individual pigments per snapshot, this leads to more than 1.4 million QM/MM calculations per solvent and temperature. As discussed already earlier,<sup>23</sup> the energy gap autocorrelation functions decay quickly, within the first 100–200 fs, and vanish within 1–2 ps. To calculate correlation functions of 2 ps length, 4 ps-long windows were employed. Using a spacing of 250 fs, there are about 1700 4 ps-long windows along the MD trajectories. The correlation functions were calculated for each window and then averaged. In previous studies<sup>23,32</sup> the correlation functions were fitted to an analytical form: a combination of exponentials and damped oscillations. Here we refrain from this procedure since the fitting introduces ambiguities. Furthermore, as previously shown, large timesteps between the energy gaps leads to overemphasized spectral densities at high frequencies.<sup>42</sup> Apparently for the present case, 5 fs time steps between energy gap values lead to a nonvanishing spectral density at high frequencies, especially when employing eq 4 rather than eq 3. To correct for this high-frequency offset, we shift the half-sided Fourier transform to vanish at high frequencies before multiplying with the prefactor in eq 4 such that the influence on the low-frequency part is negligible. This procedure has been tested for the example in ref 42, yielding very good results.

The room-temperature spectral densities determined using the procedure outlined above are shown in Figure 4 for all eight chromophores. The numerical data for these individual spectral densities are provided as Supporting Information. The spectral densities for FMO in the different solvents at ambient temperature are similar, and no systematic differences can be found. For BChls 6 and 8, the differences are somewhat larger, but once the spectral density with water as solvent is larger and once with the glycerol–water mixture. Since the two MD simulation setup with the different solvents have been constructed independently, the present findings show some robustness of the results. Examples for the spectral densities at 77 K for BChl 1 are provided in Figure 5. The spectral densities of the other chromophores behave very similarly (data not shown). Since at low temperatures the DOS of the energy gaps are already different among the monomers, the same is also true for the spectral densities. Therefore, the presented results should only be considered as examples and not as unique

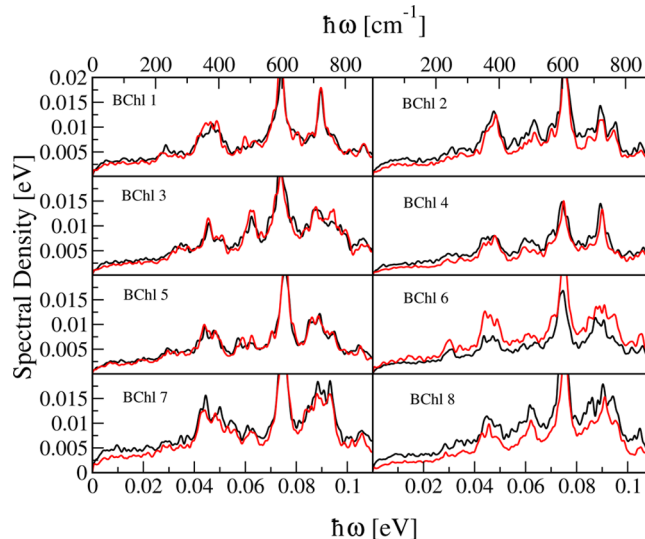


**Figure 4.** Ambient temperature spectral densities of the eight FMO BChls surrounded by water at 300 K (black) and a glycerol–water mixture at 310 K (red).

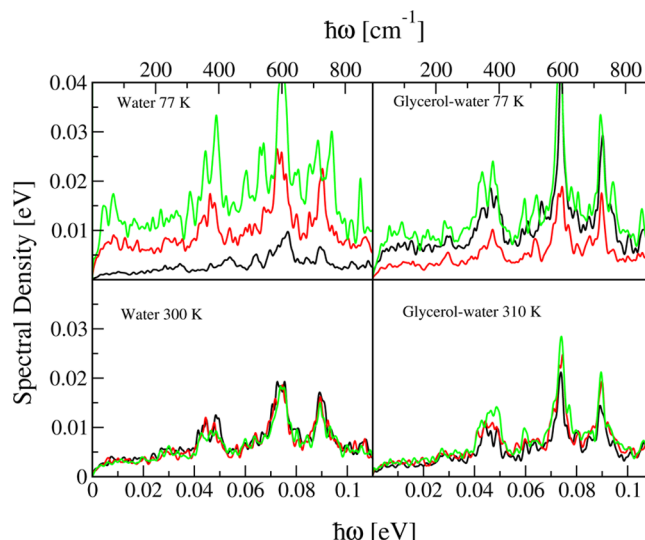


**Figure 5.** Spectral densities for BChl 1 and the three individual monomers (black, red, green) of the FMO trimer at low and ambient temperatures for the two different solvents.

results. Due to the variations in the results at 77 K, no useful statements concerning the temperature independence of the present spectral densities can be made in the present study. More analysis and much more sampling would be needed for this purpose.

A major difference to our previously reported spectral density for FMO in water at 300 K is the amplitude at low frequencies. This range of the spectral density is of particular importance since it strongly influences excitation transfer dynamics of FMO. The amplitude of the spectral densities presented herein is about a factor 2–3 smaller than the earlier results.<sup>23</sup> This difference is due to the inclusion of all the classical MD charges in the simulation rather than only those within a given, albeit large, radius. In earlier studies it was shown that neglecting the environmental charges in the energy gap calculations leads to spectral densities, which are nearly vanishing at low frequencies highlighting the importance of the environment.<sup>23</sup> In the large

frequency regime, the present spectral density is enhanced due to the altered prefactor in eq 4.

Several other spectral densities for FMO have been proposed. Adolphs and Renger estimated the electron-environment coupling based on fluorescence line narrowing spectra.<sup>43</sup> The Fleming group has proposed two other spectral densities,<sup>44,45</sup> which do not differ greatly from that of Adolphs and Renger. Furthermore, Nalbach et al.<sup>11</sup> employed the spectral density of Adolphs and Renger with the addition of a broadened single vibrational mode. Additionally, an experimental spectral density has been constructed based on a fluorescence line narrowing spectrum of FMO published by Wendling et al.<sup>28</sup> Here we use the version with the estimated Huang–Rhys factor of 0.5<sup>43</sup> with a functional form based on the original experimental data.<sup>28</sup> In these experiments the solvent was a 2:1 glycerol–water mixture, i.e., was very close to the simulated conditions. From these experiments one can only extract an average spectral density and, therefore, we plot the experimental findings together with the averages of our results in Figure 6. The experimental spectral density vanishes at

Moreover, in Figure 6 the comparison to the results Valleau et al.<sup>27</sup> is shown for the spectral densities averaged over all pigments. In principle, the procedure to obtain the spectral densities by Valleau et al.<sup>27</sup> is very similar to the one used in the present study. At the same time, many details are different such as the force fields used (AMBER vs CHARMM), the quantum chemistry approach (TDDFT vs ZINDO/S-CIS), and that in the present study a much larger number of snapshots have been taken into account, which was possible due to the computationally cheaper method to determine the energy gaps. Clear differences between the results by Valleau et al.<sup>27</sup> and our spectral densities are visible and have to be resolved in future studies. However, the difference between the spectral densities is now much smaller than in the previous versions of the spectral densities by the same groups<sup>23,25</sup> and they are closer to the experimentally extracted data.

Previously we reported calculated linear and two-dimensional absorption spectra of FMO in water at room temperature.<sup>22</sup> Neither calculation, however, included static disorder, i.e., slow, large-scale structural changes of the protein. In these previous ensemble-averaged wave packet calculations, no oscillations were found at ambient temperatures, neither in the excited state population dynamics nor in the 2D spectra. The results reported here require that these calculations be redone using the energy-gap trajectories. Since the present spectral densities are much closer to the one of Adolphs and Renger<sup>43</sup> compared to our previous calculations,<sup>22</sup> it is expected that the oscillations found in time-resolved 2D absorption spectroscopy experiments will likely be recovered. Work in this direction is in progress.

In conclusion, the present results show spectral densities using pure water or a glycerol–water mixture at ambient temperature. These spectral densities are similar to experimental findings<sup>28</sup> in the low-frequency regime. A similar improvement in spectral density calculations has recently also been achieved by Valleau et al.<sup>27</sup> The two existing sets of spectral densities for the FMO complex based on atomistic simulations are now much closer than before, although they arise from somewhat different procedures. As mentioned above, these first-principle based spectral densities can now be employed to better understand the reasons of the experimentally observed long-lived coherence in FMO.<sup>5–7</sup> Especially the reduction of the spectral density in the low-frequency regime compared to our previous results<sup>23</sup> will lead to significant changes in the exciton dynamics and therefore the corresponding 2D spectra. Moreover, it is clear from the present and previous studies<sup>22,23</sup> that the electrostatic interactions of the pigments with their environment is of key importance. This was especially seen in ref 22 by performing the QM calculations along the MD trajectory without the MM coupling, leading to strongly reduced spectral densities. Moreover, small but noticeable differences between the different environments water or a glycerol–water mixture were observed. Moreover, MD simulation of FMO shows a possible occurrence of static disorder in low temperature, which can be interpreted as larger time scales mainly due to the closely packed structure.

## ASSOCIATED CONTENT

### Supporting Information

The spectral densities detailed in this letter are supplied. This material is available free of charge via the Internet at <http://pubs.acs.org/>.

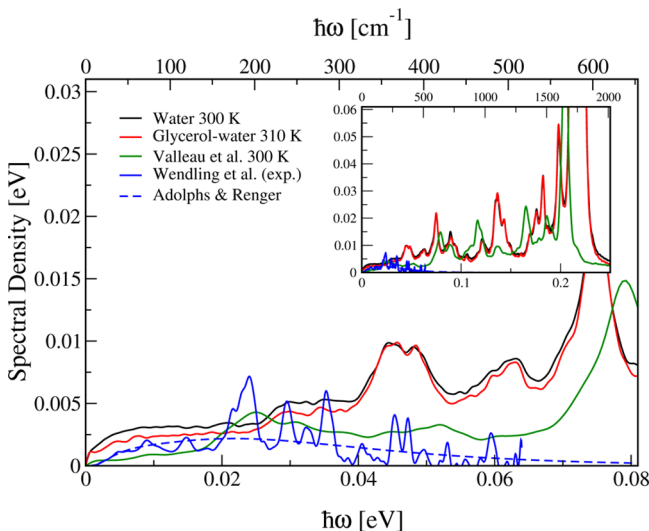


**Figure 6.** Comparison of the present spectral densities with the experimental results by Wendling et al.,<sup>28</sup> the simplified spectral density by Adolphs and Renger,<sup>43</sup> and the simulation results by Valleau et al.<sup>27</sup> The inset shows a larger frequency range.

higher frequencies, possibly due to the insensitivity of the fluorescence line narrowing procedure used by Wendling et al. in the high-frequency range. At low frequencies the experimental spectral density is below our present results. It is interesting to see that the number and widths of peaks in the experimental and theoretical spectral densities are very similar. The calculated spectral densities are missing the peak near 0.023 eV but show some reminiscent features of the peaks near 0.030 and 0.035 eV as well as the double peak structure near 0.047 eV, although the amplitudes are rather different. A direct determination of the experimental spectral density would permit a more detailed comparison with the present theoretical calculations. Nevertheless, the structure of the theoretical spectral density is supported by the experimental findings, in particular, the feature that the spectral density is not just a smooth function as in the case of the Drude form often assumed.

## AUTHOR INFORMATION

### Corresponding Author

\*E-mail: u.kleinekathofer@jacobs-university.de.

### Author Contributions

<sup>†</sup>Contributed equally to this work.

### Notes

The authors declare no competing financial interest.

## ACKNOWLEDGMENTS

We are grateful to Tönu Pullerits for providing the experimental data of ref 28, as well as to Stéphanie Valneau, Alexander Eisfeld, and Alan Aspuru-Guzik for sharing their results previous to publication. This work has been supported by Grant KL 1299/12-1 of the Deutsche Forschungsgemeinschaft (DFG), the National Institute of Health (NIH), and the National Science Foundation (NSF). Funding for J.S. and K.S. was provided by NSF Grants MCB-0744057 and PHY0822613 and NIH Grant P41-RR05969.

## REFERENCES

- (1) Wen, J.; Zhang, H.; Gross, M. L.; Blankenship, R. E. Membrane orientation of the FMO antenna protein from *Chlorobaculum tepidum* as determined by mass spectrometry-based footprinting. *Proc. Natl. Acad. Sci. U.S.A.* **2009**, *106*, 6134–6139.
- (2) Matthews, B. W.; Fenna, R. E.; Bolognesi, M. C.; Schmid, M. F.; Olson, J. M. Structure of a bacteriochlorophyll a-protein from the green photosynthetic bacterium *Prosthecochloris aestuarii*. *J. Mol. Biol.* **1979**, *131*, 259–265.
- (3) Tronrud, D. E.; Schmid, M. F.; Matthews, B. W. Structure and X-ray amino acid sequence of a bacteriochlorophyll a protein from *Prosthecochloris aestuarii* refined at 1.9 Å resolution. *J. Mol. Biol.* **1986**, *188*, 443–444.
- (4) Tronrud, D. E.; Wen, J.; Gay, L.; Blankenship, R. E. The structural basis for the difference in absorbance spectra for the FMO antenna protein from various green sulfur bacteria. *Photosynth. Res.* **2009**, *100*, 79–87.
- (5) Brixner, T.; Stenger, J.; Vaswani, H. M.; Cho, M.; Blankenship, R. E.; Fleming, G. R. Two-dimensional spectroscopy of electronic couplings in photosynthesis. *Nature* **2005**, *434*, 625–628.
- (6) Engel, G. S.; Calhoun, T. R.; Read, E. L.; Ahn, T. K.; Mancal, T.; Cheng, Y. C.; Blankenship, R. E.; Fleming, G. R. Evidence for wavelike energy transfer through quantum coherence in photosynthetic systems. *Nature* **2007**, *446*, 782–786.
- (7) Panitchayangkoon, G.; Hayes, D.; Fransted, K. A.; Caram, J. R.; Harel, E.; Wen, J.; Blankenship, R. E.; Engel, G. S. Long-lived quantum coherence in photosynthetic complexes at physiological temperature. *Proc. Natl. Acad. Sci. U.S.A.* **2010**, *107*, 12766–12770.
- (8) Collini, E.; Wong, C. Y.; Wilk, K. E.; Curmi, P. M.; Brumer, P.; Scholes, G. D. Coherently wired light-harvesting in photosynthetic marine algae at ambient temperature. *Nature* **2010**, *463*, 644–647.
- (9) Collini, E.; Scholes, G. D. Coherent intrachain energy migration in a conjugated polymer at room temperature. *Science* **2009**, *323*, 369–373.
- (10) Moix, J.; Wu, J.; Huo, P.; Coker, D.; Cao, J. Efficient energy transfer in light-harvesting systems, III: The influence of the eighth bacteriochlorophyll on the dynamics and efficiency in FMO. *J. Phys. Chem. Lett.* **2011**, *2*, 3045–3052.
- (11) Nalbach, P.; Braun, D.; Thorwart, M. Exciton transfer dynamics and quantumness of energy transfer in the Fenna–Matthews–Olson complex. *Phys. Rev. E* **2011**, *84*, 041926.
- (12) Curutchet, C.; Kongsted, J.; Munoz Losa, A.; Hossein Nejad, H.; Scholes, G. D.; Mennucci, B. Photosynthetic light-harvesting is tuned by the heterogeneous polarizable environment of the protein. *J. Am. Chem. Soc.* **2011**, *133*, 3078–3084.
- (13) Nalbach, P.; Thorwart, M. The role of discrete molecular modes in the coherent exciton dynamics in FMO. *J. Phys. B: At., Mol. Opt. Phys.* **2012**, *45*, 154009.
- (14) Ishizaki, A.; Fleming, G. R. Quantum coherence in photosynthetic light harvesting. *Annu. Rev. Condens. Matter Phys.* **2012**, *3*, 333–361.
- (15) Mühlbacher, L.; Kleinekathöfer, U. Preparational effects on the excitation energy transfer in the FMO complex. *J. Phys. Chem. B* **2012**, *116*, 3900–3906.
- (16) Dijkstra, A. G.; Tanimura, Y. The role of the environment time scale in light-harvesting efficiency and coherent oscillations. *New J. Phys.* **2012**, *14*, 073027.
- (17) Kolli, A.; O'Reilly, E. J.; Scholes, G. D.; Olaya Castro, A. The fundamental role of quantized vibrations in coherent light harvesting by cryptophyte algae. *J. Chem. Phys.* **2012**, *137*, 174109–15.
- (18) Kreisbeck, C.; Kramer, T. Long-lived electronic coherence in dissipative exciton dynamics of light-harvesting complexes. *J. Phys. Chem. Lett.* **2012**, *3*, 2828–2833.
- (19) Pachon, L. A.; Brumer, P. Computational methodologies and physical insights into electronic energy transfer in photosynthetic light-harvesting complexes. *Phys. Chem. Chem. Phys.* **2012**, *14*, 10094–10108.
- (20) Christansson, N.; Kauffmann, H. F.; Pullerits, T.; Mančal, T. Origin of long-lived coherences in light-harvesting complexes. *J. Phys. Chem. B* **2012**, *116*, 7449–7454.
- (21) Olbrich, C.; Strümpfer, J.; Schulten, K.; Kleinekathöfer, U. Quest for spatially correlated fluctuations in the FMO light-harvesting complex. *J. Phys. Chem. B* **2011**, *115*, 758–764.
- (22) Olbrich, C.; Jansen, T. L. C.; Liebers, J.; Aghtar, M.; Strümpfer, J.; Schulten, K.; Knoester, J.; Kleinekathöfer, U. From atomistic modeling to excitation dynamics and two-dimensional spectra of the FMO light-harvesting complex. *J. Phys. Chem. B* **2011**, *115*, 8609–8621.
- (23) Olbrich, C.; Strümpfer, J.; Schulten, K.; Kleinekathöfer, U. Theory and simulation of the environmental effects on FMO electronic transitions. *J. Phys. Chem. Lett.* **2011**, *2*, 1771–1776.
- (24) Olbrich, C.; Kleinekathöfer, U. From atomistic modeling to electronic properties of light-harvesting systems. In *Quantum Efficiency in Complex Systems, Part II: From Molecular Aggregates to Organic Solar Cells*; Elsevier Science: Burlington, MA, 2011; pp 83–114.
- (25) Shim, S.; Rebentrost, P.; Valneau, S.; Aspuru Guzik, A. Atomistic study of the long-lived quantum coherences in the Fenna–Matthew–Olson complex. *Biophys. J.* **2012**, *102*, 649–660.
- (26) Kim, H. W.; Kelly, A.; Park, J. W.; Rhee, Y. M. All-atom semiclassical dynamics study of quantum coherence in photosynthetic Fenna–Matthews–Olson complex. *J. Am. Chem. Soc.* **2012**, *134*, 11640–11651.
- (27) Valneau, S.; Eisfeld, A.; Aspuru Guzik, A. On the alternatives for bath correlators and spectral densities from mixed quantum-classical simulations. *J. Chem. Phys.* **2012**, *137*, 224103–13.
- (28) Wendling, M.; Pullerits, T.; Przyjalgowski, M. A.; Vulto, S. I. E.; Artsma, T. J.; Grondelle, R. v.; Amerongen, H. v. Electron-vibrational coupling in the Fenna–Matthews–Olson complex of *Prosthecochloris aestuarii* determined by temperature-dependent absorption and fluorescence line-narrowing measurement. *J. Phys. Chem. B* **2000**, *104*, 5825–5831.
- (29) Heřman, P.; Kleinekathöfer, U.; Barvík, I.; Schreiber, M. Exciton scattering in light-harvesting systems of purple bacteria. *J. Lumin.* **2001**, *94&95*, 447–450.
- (30) Heřman, P.; Kleinekathöfer, U.; Barvík, I.; Schreiber, M. Influence of static and dynamic disorder on the anisotropy of emission in the ring antenna subunits of purple bacteria photosynthetic systems. *Chem. Phys.* **2002**, *275*, 1–13.
- (31) Damjanović, A.; Kosztin, I.; Kleinekathöfer, U.; Schulten, K. Excitons in a photosynthetic light-harvesting system: A combined molecular dynamics, quantum chemistry and polaron model study. *Phys. Rev. E* **2002**, *65*, 031919.

- (32) Olbrich, C.; Kleinekathöfer, U. Time-dependent atomistic view on the electronic relaxation in light-harvesting system II. *J. Phys. Chem. B* **2010**, *114*, 12427–12437.
- (33) Hatcher, E. R.; Guvench, O.; MacKerell, A. D. CHARMM additive all-atom force field for acyclic polyalcohols, acyclic carbohydrates, and inositol. *J. Chem. Theory Comput.* **2009**, *5*, 1315–1327.
- (34) Egorov, A. V.; Lyubartsev, A. P.; Laaksonen, A. Molecular dynamics simulation study of glycerol–water liquid mixtures. *J. Phys. Chem. B* **2011**, *115*, 14572–14581.
- (35) Cory, M. G.; Zerner, M. C.; Hu, X.; Schulten, K. Electronic excitations in aggregates of bacteriochlorophylls. *J. Phys. Chem. B* **1998**, *102*, 7640–7650.
- (36) Wanko, M.; Hoffmann, M.; Strodel, P.; Koslowski, A.; Thiel, W.; Neese, F.; Frauenheim, T.; Elstner, M. Calculating absorption shifts for retinal proteins: Computational challenges. *J. Phys. Chem. B* **2005**, *109*, 3606.
- (37) Alberti, S. F.; Echave, J. Theoretical study of the solvatochromism of a merocyanine dye. *Chem. Phys.* **1997**, *223*, 183–194.
- (38) Petrenko, T.; Neese, F. Analysis and prediction of absorption band shapes, fluorescence band shapes, resonance Raman intensities, and excitation profiles using the time-dependent theory of electronic spectroscopy. *J. Chem. Phys.* **2007**, *127*, 164319.
- (39) May, V.; Kühn, O. *Charge and Energy Transfer in Molecular Systems*; Wiley–VCH: Berlin, 2000.
- (40) Mercer, I. P.; Gould, I. R.; Klug, D. R. Optical properties of solvated molecules calculated by a QM/MM methods: Chlorophyll *a* and Bacteriochlorophyll *a*. *Faraday Discuss.* **1997**, *108*, 51–62.
- (41) Ceccarelli, M.; Procacci, P.; Marchi, M. An ab initio force field for the cofactors of bacterial photosynthesis. *J. Comput. Chem.* **2003**, *24*, 129–132.
- (42) Aghtar, M.; Liebers, J.; Strümpfer, J.; Schulten, K.; Kleinekathöfer, U. Juxtaposing density matrix and classical path-based wave packet dynamics. *J. Chem. Phys.* **2012**, *136*, 214101–9.
- (43) Adolphs, J.; Renger, T. How proteins trigger excitation energy transfer in the FMO complex of green sulfur bacteria. *Biophys. J.* **2006**, *91*, 2778–2797.
- (44) Cho, M.; Vaswani, H. M.; Brixner, T.; Stenger, J.; Fleming, G. R. Exciton analysis in 2D electronic spectroscopy. *J. Phys. Chem. B* **2005**, *109*, 10542–56.
- (45) Ishizaki, A.; Fleming, G. R. Theoretical examination of quantum coherence in a photosynthetic system at physiological temperature. *Proc. Natl. Acad. Sci. U.S.A.* **2009**, *106*, 17255–17260.